# Sliding-Window Multi-Anchor Fusion for UAV Localization in Urban Canyons

Po-Wei Wu, Tzu-Hao Huang, Chao-Kai Wen, *Fellow, IEEE*, and Trung Q. Duong, *Fellow, IEEE*

***Abstract*—Reliable localization of uncrewed aerial vehicles (UAVs) in dense urban canyons is challenging due to GNSS degradation and irregular radio propagation. Received signal strength (RSS) fingerprinting from existing 4G/5G cellular systems provides GNSS-free absolute positioning but still suffers from noisy and intermittent measurements, while inertial measurement units (IMUs) offer smooth relative motion estimation with accumulated drift. Conventional point-wise fusion methods, such as extended Kalman filters, are sensitive to RSS outliers and fail to exploit geometric consistency along UAV trajectories. This letter proposes a sliding-window multi-anchor fusion framework that jointly aligns IMU trajectory segments with multiple RSS fingerprint anchors within a local temporal window. By leveraging window-level geometric consistency and outlier suppression, the proposed approach improves robustness to multipath-induced RSS errors while preserving trajectory continuity under sparse anchor conditions. Simulation results in a realistic three-dimensional urban canyon environment demonstrate significantly reduced large localization errors compared with single-modality localization and point-wise fusion methods.**

***Index Terms*—UAV, Fingerprint, RSS, Sliding Window, WKNN, IMU.**

## I. Introduction

Reliable localization is essential for uncrewed aerial vehicle (UAV) operations in dense urban environments, supporting applications such as infrastructure inspection, public safety, and intelligent transportation. Under nominal open-sky conditions, global navigation satellite system (GNSS)-based localization combined with inertial sensing provides accurate positioning. In urban canyons, however, GNSS signals are often severely degraded or unavailable due to building blockage and multipath propagation. As a result, GNSS-based localization alone cannot meet the robustness requirements of low-altitude urban UAV flights, motivating resilient localization solutions for GNSS-degraded conditions.

To mitigate GNSS degradation, alternative sensing modalities have been widely explored. Inertial measurement units (IMUs) provide high-rate relative motion information without external signals but inevitably accumulate drift over time [1]. Radio-based localization methods, such as received signal strength (RSS) fingerprinting using cellular infrastructure, offer GNSS-free absolute position references [2], [3]. However, in dense urban canyons, RSS measurements are still highly sensitive to shadowing and multipath, leading to noisy and intermittent position estimates [4]. Consequently, neither IMU-only nor RSS-only localization is sufficient for stable UAV positioning in realistic urban scenarios.

A natural approach is to fuse IMU with radio-based absolute positioning. Conventional fusion methods typically rely on point-wise updates, such as extended Kalman filters (EKFs) [5]. While effective under mild noise conditions, point-wise fusion becomes fragile in urban canyons, where RSS fingerprint errors are often heavy-tailed and temporally intermittent. Erroneous updates can significantly distort the estimated state, and the resulting error may persist during periods of anchor unavailability. Moreover, point-wise fusion treats measurements independently and fails to exploit local geometric consistency along short trajectory segments.

Recent studies have explored trajectory-level or window-based fusion to improve robustness against non-Gaussian radio measurement errors, mainly focusing on indoor localization scenarios with dense and continuously available measurements [6]. In contrast, UAV localization in dense urban canyons presents fundamentally different conditions, where cellular RSS fingerprint anchors are not only noisy but also intermittent or even unavailable. These characteristics call for online and causal fusion strategies that maintain trajectory continuity while exploiting local geometric consistency whenever reliable anchors are present.

In this letter, we propose a sliding-window multi-anchor fusion (SW-MAF) framework for resilient UAV localization in dense urban canyons. Instead of correcting inertial drift using instantaneous RSS estimates, the proposed approach aggregates available RSS fingerprint anchors within a local temporal window and jointly aligns the corresponding IMU trajectory segment to these anchors. Window-level outlier suppression mitigates multipath-induced errors, while IMU propagation preserves trajectory continuity when reliable anchors are insufficient.

The proposed framework is evaluated in a realistic three-dimensional (3D) urban canyon scenario constructed from real building layouts and cellular deployments [7]. Simulation results show that the proposed sliding-window fusion significantly improves localization robustness compared with single-modality localization and point-wise fusion methods,

The work of P.-W. Wu, T.-H. Huang, and C.-K. Wen was supported in part by the National Science and Technology Council (NSTC) of Taiwan under Grants NSTC 114-2221-E-110-031-MY3 and NSTC 114-2218-E-110-006, and in part by the Sixth Generation Communication and Sensing Research Center, funded by the Higher Education SPROUT Project of the Ministry of Education (MOE) of Taiwan. The work of T. Q. Duong was supported in part by the Canada Excellence Research Chair (CERC) Program CERC-2022-00109 and in part by the Natural Sciences and Engineering Research Council of Canada (NSERC) Discovery Grant Program RGPIN-2025-04941.

P.-W. Wu, T.-H. Huang, and C.-K. Wen are with the Institute of Communications Engineering, National Sun Yat-sen University, Kaohsiung 80424, Taiwan, Email: {peter0911600929, peter94135}@gmail.com, chaokai.wen@mail.nsysu.edu.tw.

T. Q. Duong is with the Faculty of Engineering and Applied Science, Memorial University, St. John's, NL A1C 5S7, Canada, and also with the School of Electronics, Electrical Engineering and Computer Science, Queen's University Belfast, BT7 1NN Belfast, U.K. (e-mail: tduong@mun.ca.)

particularly by suppressing large localization errors under intermittent RSS conditions.

## II. Problem Setup

We study UAV localization in GNSS-degraded urban canyons, where blockage and multipath severely distort satellite signals. The UAV operates in a realistic 3D urban environment with cellular infrastructure modeled using real-world 4G/5G base-station (BS) locations and antenna orientations. At time index $k$, the UAV accesses two complementary sensing modalities with distinct error characteristics.

**RSS fingerprinting (absolute but intermittent):** Given a pre-built 3D RSS fingerprint database, the UAV measures an RSS feature vector $\mathbf{r}_k = (\mathrm{RSS}_{1,k}, \ldots, \mathrm{RSS}_{M,k})$ from $M$ BS sectors and obtains an absolute position estimate $\widehat{\mathbf{x}}_k^{\mathrm{RSS}} \in \mathbb{R}^3$ via weighted K-nearest neighbors (WKNN) matching [8], [9]. Each sector is characterized by its carrier frequency and antenna orientation. Due to shadowing and limited BS visibility, $\widehat{\mathbf{x}}_k^{\mathrm{RSS}}$ is noisy and intermittent; if all received RSS values fall below $-120$ dBm, the estimate is treated as unavailable due to low reliability.[1] Multipath propagation can also further induce large outliers.

**IMU dead reckoning (dense but drifting):** Let $\mathbf{p}_k^{\mathrm{IMU}} \in \mathbb{R}^3$ denote the dead-reckoning position obtained by integrating IMU measurements. IMU provides smooth, high-rate relative motion without relying on external signals, but accumulates drift over time due to sensor noise and bias. Consequently, IMU-only localization is locally consistent but globally unbounded in error.

These two modalities create a challenging fusion setting: RSS anchors provide absolute references but are intermittent and heavy-tailed, whereas IMU motion is continuous but drifts. A straightforward solution is point-wise fusion, such as EKF-based updates that incorporate a single RSS-based measurement at each time step [5]. However, in urban canyons, a single outlier update can significantly distort the estimated state, and the error may persist during periods of anchor unavailability. Moreover, point-wise fusion processes measurements independently and does not exploit local geometric consistency among multiple anchors observed along a short trajectory segment.

## III. Sliding-Window Multi-Anchor Fusion

To improve robustness under sparse and noisy RSS fingerprint anchors, we propose an online SW-MAF framework. The proposed method leverages both current and past observations and is therefore not strictly real-time. Instead of correcting IMU drift using instantaneous RSS estimates, SW-MAF aggregates available anchors within a local temporal window and aligns the corresponding IMU trajectory segment to these anchors. This window-level formulation reduces sensitivity to individual outliers and preserves trajectory continuity when anchors are unavailable.

[1]Although, according to 3GPP TS 36.133, RSRP measurements can be reported down to approximately $-140$ dBm, we adopt a more conservative threshold suitable for commercial applications.

Algorithm 1 summarizes the procedure. The framework consists of three components: *i)* sliding-window construction and anchor collection, *ii)* window-level outlier suppression, and *iii)* similarity alignment with IMU fallback. The fused position at time $k$ is denoted by $\widehat{\mathbf{x}}_k^{\mathrm{fused}} \in \mathbb{R}^3$.

### A. Sliding Window and Candidate Anchors

Consider a UAV trajectory indexed by $k \in \{0, 1, \ldots, T-1\}$. Let $\mathbf{p}_k^{\mathrm{IMU}}$ denote the IMU dead-reckoning position, and let $\widehat{\mathbf{x}}_k^{\mathrm{RSS}}$ denote the WKNN-based absolute position estimate when available. A sliding window of length $L$ at time $k$ is defined as

$$\mathcal{W}_k = \{\max(0, k-L+1), \ldots, k\}, \tag{1}$$

where $\max(0, k-L+1)$ returns the larger value between 0 and $k-L+1$, ensuring that the window starts from the earliest valid index. Let $\mathcal{V}_k \subseteq \mathcal{W}_k$ denote the set of indices for which RSS anchors are available:

$$\mathcal{V}_k = \left\{ i \in \mathcal{W}_k \mid \widehat{\mathbf{x}}_i^{\mathrm{RSS}} \text{ is available} \right\}. \tag{2}$$

When $|\mathcal{V}_k|$ is small, the available anchors are insufficient to constrain a stable geometric correction. Therefore, fusion is activated only when the number of retained anchors exceeds a minimum-anchor threshold $\tau$, i.e., $|\mathcal{V}_k| \geq \tau$.

### B. Window-Level Outlier Suppression

The anchor set $\{\widehat{\mathbf{x}}_i^{\mathrm{RSS}}\}_{i \in \mathcal{V}_k}$ may contain severe outliers due to multipath and shadowing. To suppress unreliable measurements, window-level anchor filtering is performed using density-based clustering in the spatial domain (i.e., DBSCAN [10]), and only the dominant cluster within the window is retained. Let $\widetilde{\mathcal{V}}_k \subseteq \mathcal{V}_k$ denote the indices belonging to the dominant cluster, and define the filtered anchor set as

$$\widetilde{\mathcal{A}}_k = \left\{ \widehat{\mathbf{x}}_i^{\mathrm{RSS}} \mid i \in \widetilde{\mathcal{V}}_k \right\}. \tag{3}$$

This window-level filtering exploits spatial consistency across multiple anchors and prevents isolated fingerprint errors from dominating the fusion.

### C. Similarity Alignment and Output

With the filtered anchors in the current window, a similarity transformation is estimated to align the IMU trajectory segment to the RSS anchors. Specifically, when $|\widetilde{\mathcal{V}}_k| \geq \tau$, the alignment is obtained by solving

$$\min_{s_k, \mathbf{R}_k, \mathbf{t}_k} \sum_{i \in \widetilde{\mathcal{V}}_k} \left\| s_k \mathbf{R}_k \mathbf{p}_i^{\mathrm{IMU}} + \mathbf{t}_k - \widehat{\mathbf{x}}_i^{\mathrm{RSS}} \right\|_2^2, \tag{4}$$

where $s_k \in \mathbb{R}$ is a scale factor, $\mathbf{R}_k \in \mathbb{R}^{3\times 3}$ is a rotation matrix, and $\mathbf{t}_k \in \mathbb{R}^3$ is a translation vector. The optimization in (4) admits a closed-form solution based on similarity Procrustes analysis, which can be efficiently computed using singular value decomposition [11]. The fused position is then given by

$$\widehat{\mathbf{x}}_k^{\mathrm{fused}} = s_k \mathbf{R}_k \mathbf{p}_k^{\mathrm{IMU}} + \mathbf{t}_k. \tag{5}$$

**Algorithm 1:** Online SW-MAF

**Input:** IMU dead-reckoning positions $\{\mathbf{p}_k^{\mathrm{IMU}}\}$, RSS-based estimates $\{\widehat{\mathbf{x}}_k^{\mathrm{RSS}}\}$, window length $L$, anchor threshold $\tau$

**Output:** Fused positions $\{\widehat{\mathbf{x}}_k^{\mathrm{fused}}\}$

Initialize $\widehat{\mathbf{x}}_0^{\mathrm{fused}} = \mathbf{x}_0$ and $(s^\star, \mathbf{R}^\star, \mathbf{t}^\star) \leftarrow \varnothing$;
**for** $k = 1$ **to** $T-1$ **do**
  Construct sliding window $\mathcal{W}_k$;
  Collect RSS anchors $\mathcal{V}_k \subseteq \mathcal{W}_k$;
  Apply window-level clustering to obtain $\widetilde{\mathcal{V}}_k$;
  **if** $|\widetilde{\mathcal{V}}_k| \geq \tau$ **then**
    Estimate $(s_k, \mathbf{R}_k, \mathbf{t}_k)$ by (4);
    $(s^\star, \mathbf{R}^\star, \mathbf{t}^\star) \leftarrow (s_k, \mathbf{R}_k, \mathbf{t}_k)$;
    $\widehat{\mathbf{x}}_k^{\mathrm{fused}} \leftarrow s_k \mathbf{R}_k \mathbf{p}_k^{\mathrm{IMU}} + \mathbf{t}_k$;
  **else**
    **if** $(s^\star, \mathbf{R}^\star, \mathbf{t}^\star)$ *exists* **then**
      $\widehat{\mathbf{x}}_k^{\mathrm{fused}} \leftarrow s^\star \mathbf{R}^\star \mathbf{p}_k^{\mathrm{IMU}} + \mathbf{t}^\star$;
    **else**
      $\widehat{\mathbf{x}}_k^{\mathrm{fused}} \leftarrow \widehat{\mathbf{x}}_{k-1}^{\mathrm{fused}} + (\mathbf{p}_k^{\mathrm{IMU}} - \mathbf{p}_{k-1}^{\mathrm{IMU}})$;

The latest valid transformation parameters are cached as $(s^\star, \mathbf{R}^\star, \mathbf{t}^\star)$ for subsequent use.

If $|\widetilde{\mathcal{V}}_k| < \tau$, the alignment is not updated. In this case, the most recent cached transformation $(s^\star, \mathbf{R}^\star, \mathbf{t}^\star)$ is reused when available as

$$\widehat{\mathbf{x}}_k^{\mathrm{fused}} = s^\star \mathbf{R}^\star \mathbf{p}_k^{\mathrm{IMU}} + \mathbf{t}^\star. \tag{6}$$

If no cached transformation exists (typically at early time indices), the trajectory is propagated using IMU increments:

$$\widehat{\mathbf{x}}_k^{\mathrm{fused}} = \widehat{\mathbf{x}}_{k-1}^{\mathrm{fused}} + \left(\mathbf{p}_k^{\mathrm{IMU}} - \mathbf{p}_{k-1}^{\mathrm{IMU}}\right). \tag{7}$$

## IV. Evaluation

This section evaluates the proposed SW-MAF framework in a realistic urban canyon scenario. We first describe the construction of the training and testing datasets, including the urban canyon environment, cellular deployment, RSS fingerprint database, and UAV trajectory generation.[2] We then assess localization performance under various sensing and fusion configurations.

The evaluation is conducted in a realistic 3D urban canyon environment constructed from the BostonTwin dataset [7]. As illustrated in Fig. 1(a), the simulated region spans $200\ \mathrm{m} \times 200\ \mathrm{m} \times 110\ \mathrm{m}$ and features dense and irregular building layouts typical of downtown areas. The UAV operates at altitudes between 10 and 120 m, covering both street-level flights and above-rooftop trajectories.

### A. Urban Canyon Environment and Cellular Deployment

Cellular infrastructure is modeled using real-world 4G and 5G BS locations and antenna orientations obtained from public databases (e.g., [12], [13]). Table I summarizes the antenna configurations at the three deployment sites. As shown in Fig. 1(b), BSs are grouped into three physical sites, each hosting multiple co-located sectors operating on different carrier frequencies and orientations. Within each site, sector orientations are listed following the original deployment order for reproducibility. In total, 18 BS antenna configurations are considered (i.e., $M = 18$), where 5G BSs employ $8 \times 8$ uniform planar arrays (UPAs) and 4G BSs employ $4 \times 4$ UPAs. The transmit power is set to $46\ \mathrm{dBm}$ following the macro-cell recommendation in 3GPP TS 38.104, and a fixed electrical downtilt of $10^\circ$ toward the ground is applied to all sectors.

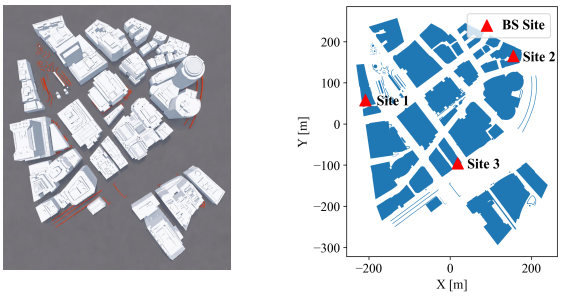


(a) 3-D urban canyon scene (b) Top-down view with BSs

Fig. 1. Simulation environment based on a realistic urban canyon scenario.

### B. RSS Propagation Characteristics and Fingerprint

RSS measurements are generated via ray tracing using Sionna [14], explicitly accounting for building-induced blockage and reflection. Fig. 2 shows representative RSS coverage maps at two UAV altitudes. The illustrated RSS maps correspond to a representative north-facing 5G sector at Site 2 (n41 band), as summarized in Table I. Lower altitudes exhibit fragmented coverage due to blockage, whereas higher altitudes provide smoother but weaker coverage. These altitude-dependent effects highlight two fundamental challenges of RSS fingerprinting in urban canyons: strong spatial irregularity and temporal instability along UAV trajectories. Consequently, RSS fingerprint-based absolute position estimates are inherently noisy and intermittent.

The RSS fingerprint database is constructed over a 3D spatial grid with a horizontal resolution of $5\ \mathrm{m} \times 5\ \mathrm{m}$ and discretized altitude levels at $1\ \mathrm{m}$ intervals, covering the entire simulated region (Fig. 1). Specifically, the fingerprint tensor has a size of $18 \times 40 \times 40 \times 110$, corresponding to 18 BS configurations, $40 \times 40$ horizontal grid points, and 110 altitude levels.

### C. Trajectory Generation and Anchor Sparsity

UAV trajectories are generated using sampling-based motion planning and smoothing techniques to ensure collision-free and realistic flight paths. Specifically, probabilistic roadmap (PRM) planning and spline-based trajectory smoothing are employed, following standard practices in UAV navigation and robotics [15]. A total of 3,000 trajectories are generated, each exceeding $150\ \mathrm{m}$ in length. For localization, each trajectory is uniformly resampled into 50 discrete time samples, defining the temporal resolution for both RSS fingerprinting and IMU

[2]The source code and datasets used in this letter are publicly available at https://github.com/powei0623/UC-OFUT

TABLE I
CELLULAR BS CONFIGURATIONS ACROSS THREE DEPLOYMENT SITES.

| Site | System | Band | DL Freq. (GHz) | Orientation |
|---|---|---|---|---|
| 1 | 5G | n41 | 2.51–2.62 | $\{173°, 2°, 183°, 358°\}$ |
| 1 | 4G | B2/B66 | 1.95 / 2.14 | $\{113°, 118°\}$ |
| 2 | 5G | n41 | 2.51–2.60 | $\{185°, 178°, 185°, 1°\}^{\dagger}$ |
| 2 | 4G | B2/B66 | 1.95 / 2.14 | $\{235°, 239°\}$ |
| 3 | 4G | B2 | 1.95 | $\{1°, 121°, 241°\}$ |
| 3 | 4G | B66 | 2.14 | $\{1°, 121°, 241°\}$ |

$^{\dagger}$ Two 5G sectors at Site 2 share the same nominal azimuth.

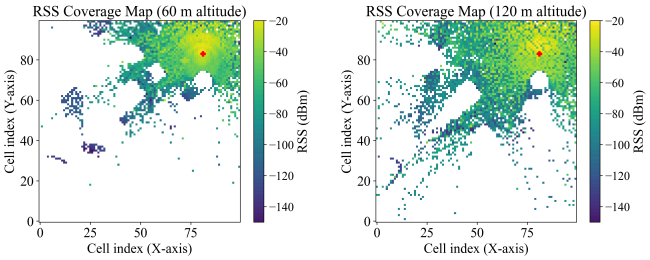


(a) 60 m altitude (b) 120 m altitude

Fig. 2. Representative RSS coverage maps of a north-facing 5G sector (n41 band) at Site 2, evaluated at two different UAV altitudes.

propagation. Due to shadowing and limited BS visibility, RSS fingerprint-based absolute positioning is highly intermittent. When all received RSS values fall below $-120$ dBm, the corresponding sample is treated as unlocalizable and excluded from absolute positioning. Across all trajectories, an average of 22.65 out of 50 samples yield valid WKNN-based position estimates, with the minimum and maximum numbers being 2 and 44, respectively.

### D. IMU Error Model and Drift Behavior

IMU measurements provide dense relative motion information but inevitably suffer from drift accumulation over time. Since the simulated UAV flights are confined to a relatively short-range region, an IMU with moderate-grade error characteristics would typically exhibit limited drift over a short-range trajectory, as shown in Fig. 3(a). To enable a meaningful evaluation of fusion robustness, an amplified IMU error model is therefore adopted.

Fig. 3 compares representative IMU-only trajectories under nominal and amplified IMU error models. With amplified errors, pronounced inertial drift is observed even within limited flight distances, emulating the error characteristics of long-duration inertial navigation. This design choice allows the proposed fusion algorithm to be evaluated more efficiently, without requiring the simulation of excessively long trajectories.

### E. Localization Performance

We compare the proposed method with four baseline localization strategies: WKNN-only, IMU-only, EKF-based point-wise fusion, and SW-MAF without outlier filtering (no OF). The results are summarized in Table II, where the proposed SW-MAF with window-level outlier suppression achieves the best overall performance, reducing the mean localization error to 21.95 m and substantially improving both RMSE and $P_{95}$ compared with all baselines. A representative trajectory

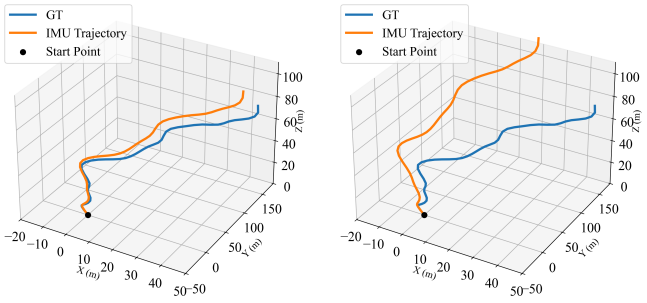


(a) Nominal IMU error model (b) Amplified IMU error model

Fig. 3. Comparison between ground-truth (GT) and IMU trajectories under (a) nominal IMU error model, and (b) amplified IMU error model.

TABLE II
LOCALIZATION ERROR STATISTICS FOR DIFFERENT POSITIONING STRATEGIES

| Method | Mean (m) | RMSE (m) | $P_{68}$ (m) | $P_{95}$ (m) |
|---|---|---|---|---|
| WKNN-only | 52.07 | 66.90 | 70.48 | 129.72 |
| IMU-only | 38.96 | 51.30 | 53.31 | 101.14 |
| SW-MAF (no OF) | 30.76 | 58.84 | 31.18 | 89.48 |
| SW-MAF | **21.95** | **33.55** | **23.55** | **73.01** |
| EKF | 45.66 | 63.52 | 51.83 | 123.11 |
| SW-MAF (unk.) | 26.51 | 37.46 | 28.63 | 78.91 |

comparison is shown in Fig. 4. IMU-only localization produces smooth trajectories but exhibits significant accumulated drift due to the absence of absolute position correction (Fig. 4(a)). WKNN-only localization relies on instantaneous RSS measurements and yields scattered, temporally discontinuous estimates with noticeable outliers (Fig. 4(b)). EKF-based fusion partially corrects inertial drift but remains sensitive to erroneous RSS updates because of its point-wise update mechanism (Fig. 4(c)). In contrast, the proposed sliding-window alignment jointly exploits IMU relative motion and multiple RSS fingerprint anchors within a local temporal window, yielding a trajectory that closely follows the ground truth while preserving temporal continuity.

The cumulative distribution functions (CDFs) of localization error are shown in Fig. 5. WKNN-only localization exhibits heavy-tailed error distributions due to multipath-induced outliers, while IMU-only suffers from unbounded drift. EKF-based fusion reduces the median error but remains ineffective in suppressing large tail errors. The SW-MAF variant without outlier filtering alleviates drift but still exhibits pronounced tail errors due to residual outliers.

For evaluation consistency, the IMU-only baseline is initialized at the true starting position to isolate drift accumulation from global offset effects. All methods are evaluated under the same initialization condition. Notably, SW-MAF does not rely on knowledge of the true starting position. As reported in the last row of Table II, SW-MAF with an unknown starting position achieves comparable performance, with only a marginal performance difference relative to the initialized case.

The impact of the minimum-anchor threshold $\tau$ is reported in Table III. When $\tau$ is too small, alignment may be triggered by insufficient or unreliable anchors, increasing sensitivity to residual outliers. Conversely, an excessively large $\tau$ delays

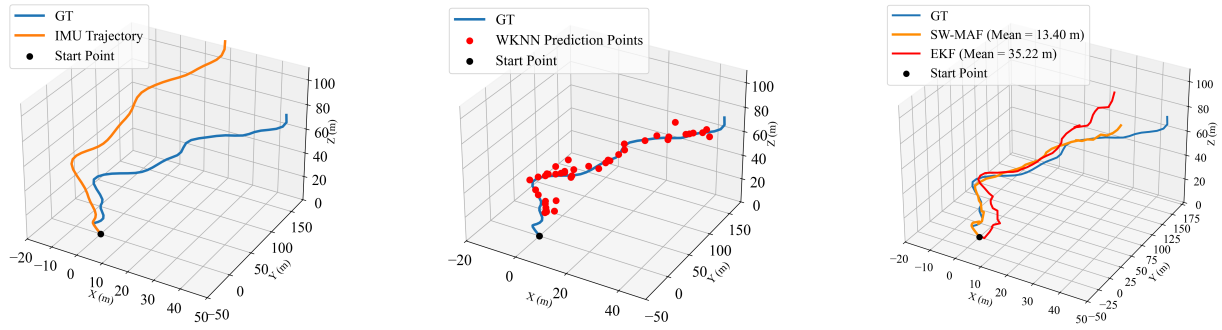


(a) IMU-only (b) WKNN-only (c) SW-MAF vs. EKF

Fig. 4. Trajectory-level comparison of different localization strategies for a representative UAV path.

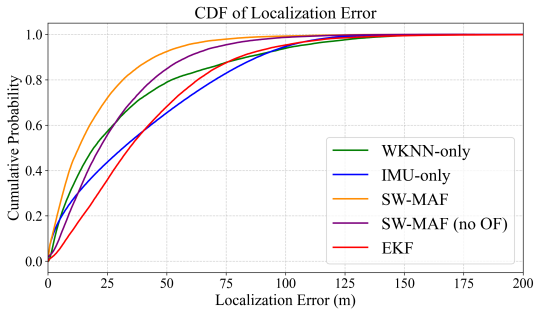


Fig. 5. CDFs of localization error under different positioning strategies.

TABLE III
IMPACT OF THE SLIDING WINDOW ACTIVATION THRESHOLD ON LOCALIZATION PERFORMANCE

| $\tau$ | Mean (m) | RMSE (m) | $P_{68}$ (m) | $P_{95}$ (m) |
|---|---|---|---|---|
| 1 | 22.23 | 35.37 | 23.50 | 73.30 |
| 6 | 21.95 | 33.55 | 23.55 | 73.01 |
| 15 | 26.28 | 37.14 | 30.42 | 81.67 |

alignment activation, resulting in prolonged IMU propagation and increased drift before correction. Based on the results in Table III, $\tau = 6$ provides a favorable balance between robustness and responsiveness and is adopted in this work. The sliding-window length $L$ affects fusion performance. Short windows yield insufficient geometric constraints, while larger windows provide diminishing gains. Localization performance stabilizes around $L \approx 30$; considering the increased computational cost and latency, $L = 35$ is adopted as a trade-off between robustness and efficiency. Future work may consider adaptive selection of the $\tau$ and $L$ based on signal quality or anchor density.

## V. Conclusion

This letter investigated UAV localization in dense urban canyons, where GNSS signals are unreliable and radio measurements are intermittent and affected by multipath. To address this challenge, we proposed an online SW-MAF framework that integrates RSS fingerprint anchors with IMU-based relative motion at the trajectory level. By replacing instantaneous corrections with window-level geometric alignment, the proposed method exploits local temporal consistency while mitigating the impact of heavy-tailed RSS outliers. Window-level outlier suppression bounds large localization errors, while IMU propagation preserves trajectory continuity during anchor outages. Rather than targeting centimeter-level accuracy, SW-MAF is designed as a resilient fallback localization solution for GNSS-degraded urban operations. Simulation results in a realistic 3D urban canyon scenario show that the proposed framework suppresses tail errors and maintains bounded localization performance under intermittent RSS conditions, offering a practical alternative to point-wise fusion during GNSS outages.

## References

[1] Y. Chang, Y. Cheng, U. Manzoor, and J. C. Murray, "A review of UAV autonomous navigation in GPS-denied environments," *Robotics and Autonomous Systems*, vol. 170, p. 104533, 2023.
[2] F. Mogyorósi *et al.*, "Positioning in 5G and 6G networks—a survey," *Sensors*, vol. 22, no. 13, p. 4757, 2022.
[3] Z. Hu, X. Chen, Z. Zhou, and S. Mumtaz, "Localization with cellular signal RSRP fingerprint of multiband and multicell," *IEEE Journal on Selected Areas in Communications*, vol. 42, no. 9, pp. 2380–2394, 2024.
[4] Q. Wu, G. Chuai, and W. Gao, "A fingerprint database construction method based on universal Kriging interpolation for outdoor localization," in *2020 IEEE/CIC International Conference on Communications in China (ICCC)*, 2020, pp. 46–51.
[5] Y. Zhuang *et al.*, "Multi-sensor integrated navigation/positioning systems using data fusion: From analytics-based to learning-based approaches," *Information Fusion*, 2023.
[6] L. Zhang, J. Ma, Y. Liu, L. Duan, Y. Liang, and Y. Lu, "A Wi-Fi/PDR fusion localization method based on genetic algorithm global optimization," *Sensors*, vol. 25, no. 24, 2025.
[7] "BostonTwin: High-fidelity urban digital twin," [Online]. Available: https://github.com/wineslab/boston_twin, 2024.
[8] M. Youssef and A. Agrawala, "The horus WLAN location determination system," *Wireless Networks*, vol. 14, pp. 357–374, 2008.
[9] K. Kaemarungsi and P. Krishnamurthy, "Properties of indoor received signal strength for wlan location fingerprinting," *MobiQuitous*, 2004.
[10] M. Ester, H.-P. Kriegel, J. Sander, and X. Xu, "A density-based algorithm for discovering clusters in large spatial databases with noise," in *Proceedings of the 2nd International Conference on Knowledge Discovery and Data Mining (KDD)*, 1996, pp. 226–231.
[11] S. Umeyama, "Least-squares estimation of transformation parameters between two point patterns," *IEEE Transactions on Pattern Analysis and Machine Intelligence*, vol. 13, no. 4, pp. 376–380, 1991.
[12] "CellMapper," [Online]. Available: https://www.cellmapper.net/map, 2025.
[13] "FCC Antenna Structure Registration (ASR)," [Online]. Available: https://wireless2.fcc.gov/UlsApp/AsrSearch/asrRegistrationSearch.jsp, 2025.
[14] J. Hoydis, S. Cammerer, F. A. Aoudia, A. Vem, N. Binder, G. Marcus, and A. Keller, "Sionna: An open-source library for next-generation physical layer research," arXiv:2203.11854, 2023, [Online]. Available: https://arxiv.org/abs/2203.11854.
[15] "PythonRobotics: A python robotics algorithms implementation," [Online]. Available: https://github.com/pgh79/PythonRobotics-master, 2025.